Triangular Spin-Orbit-Coupled Lattice with Strong Coulomb Correlations: Sn Atoms on a SiC(0001) Substrate

S. Glass,[1] G. Li,[2] F. Adler,[1] J. Aulbach,[1] A. Fleszar,[2] R. Thomale,[2] W. Hanke,[2] R. Claessen,[1] and J. Schäfer[1,*]
[1]*Physikalisches Institut and Röntgen Research Center for Complex Material Systems, Universität Würzburg, 97074 Würzburg, Germany*
[2]*Institut für Theoretische Physik und Astrophysik, Universität Würzburg, 97074 Würzburg, Germany*
(Received 19 January 2015; revised manuscript received 23 April 2015; published 18 June 2015)

Two-dimensional (2D) atom lattices provide model setups with Coulomb correlations that induce competing ground states. Here, SiC emerges as a wide-gap substrate with reduced screening. We report the first artificial high-Z atom lattice on SiC(0001) by Sn adatoms, based on experimental realization and theoretical modeling. Density-functional theory of our triangular structure model closely reproduces the scanning tunneling microscopy. Photoemission data show a deeply gapped state (~2 eV gap), and, based on our calculations including dynamic mean-field theory, we argue that this reflects a pronounced Mott-insulating scenario. We also find indications that the system is susceptible to antiferromagnetic superstructures. Such artificial lattices on SiC(0001) thus offer a novel platform for coexisting Coulomb correlations and spin-orbit coupling, with bearing for unusual magnetic phases and proposed topological quantum states of matter.

DOI: 10.1103/PhysRevLett.114.247602 PACS numbers: 79.60.Dp, 68.37.Ef, 71.15.Mb, 71.27.+a

Electron correlations in atom lattices.—Understanding and controlling the wealth of physical phenomena in two-dimensional (2D) electron systems hosted in atomic layers is of high interest for fundamental research, as well as for low-dimensional devices. Of particular importance are electronic correlations: Because of the reduced screening in 2D, the electrons can experience strong on-site Coulomb repulsion. A case in point are low-coverage phases of metals on semiconductor substrates. These can form various self-assembled lattices, with key examples including the triangular $(\sqrt{3}\times\sqrt{3})$ reconstructions on Si(111) and Ge(111) with 1/3 monolayer (ML) of Sn atoms [1,2]. In these cases, half-filled surface dangling bonds (DB) result, so one would expect a metallic band, i.e., a 2D electron gas (2DEG). However, a Mott-Hubbard insulating situation is found [1,2], where the on-site repulsion U splits occupied and unoccupied states by about this energy U. Moreover, the localized DB spins must arrange relative to each other, so that magnetic ordering is an expected consequence. Indeed, for Sn/Si(111) the evidence argues for collinear antiferromagnetism (AFM) [3].

An additional effect is the *spin-orbit coupling* (SOC), which becomes significant for high atomic number Z yet also depends on the surface atomic geometry. It leads to a spin splitting of the bands, detectable in the Fermi surface as spin texture even for uncorrelated 2DEGs [4]. When strong correlations and SOC coexist, e.g., correlation-driven magnetic order can be modified [5,6]. A variety of phases, extending from spin-orbit-coupled Mott insulators to specific cases such as topological Mott insulators, Weyl semimetals, or spin liquids can be expected [7].

For conquering this phase diagram as a function of *electron correlation* and *SOC strength*, an important handle is the substrate, as it will affect screening and hopping, and possibly also the SOC. Looking beyond the conventional semiconductor substrates Si and Ge, SiC offers a wide band gap of 3.2 eV (4H-SiC at 300 K), an almost fivefold increase over Ge (0.7 eV). Thus, for surface adatoms one must expect a strongly suppressed screening, which favors strong Coulomb repulsion U.

A promising agenda thus is to place a high-Z atom array on top of SiC. To date, this has not been achieved experimentally, because of poor quality of the substrate surface, which is inert against chemical treatments. Hydrogen gas phase etching makes the surface tractable, and graphene can be grown [8]. Still, a tremendous hurdle for growth of artificial adatoms is the persistent H termination. Its desorption at ~800 °C results in an unwanted intrinsic Si-$(\sqrt{3}\times\sqrt{3})$ reconstruction [9].

In this Letter, we report the first realization as well as experimental and theoretical characterization of a Sn atom lattice on SiC(0001). Scanning tunneling microscopy (STM) of the $(\sqrt{3}\times\sqrt{3})$-triangular lattice is reproduced by density-functional theory (DFT) modeling of the structure. In photoemission we find a large energy gap of ~2 eV and give arguments that the SiC substrate fosters this effect via large Coulomb repulsion combined with suppressed electron hopping. A subtle interplay of magnetic and charge order appears likely in this new type of spin-orbit Mott insulator, which is a leap forward into the SOC-U phase diagram for surface systems.

Technological approach.—The substrates, Si-face 4H-SiC(0001) with n doping (conductivity ~0.05 Ohmcm),

were chemically cleaned prior to loading into ultrahigh vacuum. *In situ*, they have been etched in a H gas phase process (details described elsewhere [10]). This removes the polishing damage, which cannot be achieved by wet chemistry alone. As a result, the substrates exhibit large smooth terraces, H-passivated in a (1×1) pattern. Subsequent deposition of Sn was achieved in a novel *counterflow* approach, at a substrate temperature of ~750 °C. Thereby, H gradually desorbs from the surface while, due to the immediate supply of Sn atoms, formation of the metal overlayer in the submonolayer regime can take place. A postanneal for several minutes then leads to a well-ordered lattice in $(\sqrt{3} \times \sqrt{3})$ reconstruction, observed in low-energy electron diffraction (LEED).

Structure of the adatom lattice.—The plain SiC(0001) surface, illustrated in Fig. 1(a), is a buckled Si-C bilayer, which (for the substrate "Si face") carries Si atoms on top. In both the unreconstructed DB case as well as the H-passivated case, the surface has a (1×1) periodicity. The situation changes after adsorption of Sn on the H-free DB surface, where we experimentally find the $(\sqrt{3}\times\sqrt{3})$ reconstruction. Figure 1(b) depicts the corresponding triangular LEED pattern and the large-area Sn coverage seen by STM. One also observes domain boundary lines and point defects, captured in close-up STM images Figs. 1(c) and 1(d), respectively.

The domain boundaries can be explained as registry shifts, where the $(\sqrt{3}\times\sqrt{3})$ unit cell is shifted by one Si atom to the side. This leaves a trenchlike fault line, with three possible directions (separation 120°), as observed in Figs. 1(b) and 1(c). Characteristic point defects are observed in Fig. 1(d) (*A*, ring of bright atoms; *B*, single hole; *C*, single bright atom), which are well known from the "cousin" system $(\sqrt{3} \times \sqrt{3})$-Sn/Si(111), where missing atoms or exchange with the substrate is discussed [1].

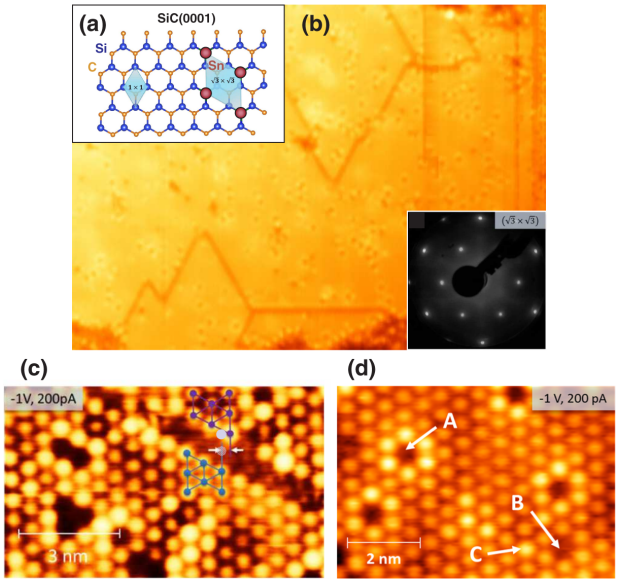

FIG. 1 (color online). (a) Schematic of the topmost buckled bilayer of the Si face of SiC(0001), covered by a $(\sqrt{3} \times \sqrt{3})$-Sn reconstruction. (b) LEED image (inset) and STM overview (−1.5 V, 100 pA, 60×42 nm, 300 K) of a $(\sqrt{3}\times\sqrt{3})$-Sn/SiC lattice. (c) Close-up of a registry shift with respect to the substrate. (d) Characteristic point defects, as discussed in the text.

For establishing a structural model of our system, we refer to key findings: (i) From x-ray photoelectron spectroscopy of the Sn and Si core levels, we determine a coverage of ~0.3 ML. This is closest to the numerical fraction 1/3 ML, as in the triangular lattice, and excludes phases with 2/3 ML or higher. (ii) The STM shows a fully coated $(\sqrt{3} \times \sqrt{3})$ surface and, in conjunction with the 1/3 ML coverage, can be explained only by a *triangular lattice*, while excluding a honeycomb (2/3 ML) or trimer (1 ML) situation.

Density-functional modeling.—This Sn/4*H*-SiC(0001)-$\sqrt{3} \times \sqrt{3}$ system is modeled in DFT by a slab of three SiC bilayers and Sn adatoms with 1/3 ML coverage on the Si face (bottom C face H-saturated). The projector-augmented-wave method in the Vienna *ab initio* simulation package (VASP) [11] within the local density approximation (LDA) was adopted [12]. SOC was included as a second variational process.

Sn is found to be energetically strongly favored when staying at the T_4 position (not H_3 or T_1) on the underlying Si layer; see total energies in Table S-I [13] and the structure model in Fig. 2(a). This is consistent with the large number of $(\sqrt{3} \times \sqrt{3})$ systems of Sn or Pb on Si(111) and Ge(111) at

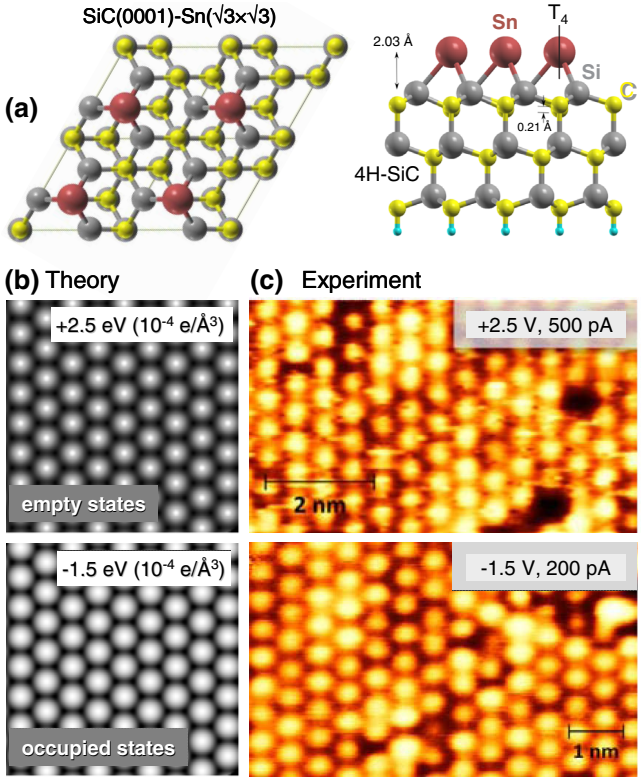

FIG. 2 (color online). (a) Structure model for DFT modeling, with Sn in T_4 sites on 4*H*-SiC(0001) (top and side view). (b) Simulated STM images, and (c) experimental STM images (300 K), for empty and occupied states, respectively. Close agreement is achieved for the whole range of tunneling parameters.

1/3 ML, where the adatoms were always found to reside on T_4 sites (systems overview in Table S-II [13]).

STM images have been simulated by the Tersoff-Hamann approximation [14], where the tunneling current depends only on the local density of states (LDOS) of the surface. Isosurfaces of the energy-integrated LDOS thus mimic measurements at fixed bias and current; see Fig. 2(b) for occupied and empty states, respectively. Regardless of the bias, the pattern is of triangular character without further substructure. Comparing to experimental STM, from a series of bias values we have compiled images in Fig. 2(c) at −1.5 (occupied states) and +2.5 V (unoccupied states). For all bias values, we find a triangular pattern with circular elevations (small deviations ascribed to the tip). Importantly, we never observe a change of pattern (e.g., honeycomb rings or trimers) that would result from a different structure.

Electronic properties.—The DFT approach also provides the electron bands including SOC, plotted in Fig. 3(a). The calculations predict a metallic ground state with a half-filled narrow DB band, situated in a large band gap, and separated from the valence band by ∼1.2 eV and the conduction band by ∼1.8 eV. Two further narrow surface bands are found in the ∼ 1.3–1.6 eV region below E_F.

The metallic band, enlarged in Fig. 3(b), is characterized by (i) a very small band width of only 0.29 eV, relating to Sn p_z orbitals hybridized with the first SiC bilayer, and (ii) a substantial SOC splitting, with maxima shifted in momentum away from the Γ point. If we characterize the SOC strength by referencing the largest SOC energy splitting to the total bandwidth, we find it amounts to 13.7% in Sn/SiC(0001), which is more than twice that of Sn/Si(111), which is only 6%.

The experimental *spectral function* has been determined by ultraviolet k-integrated photoemission ($h\nu = 21.2$ eV, resolution 10 meV), as shown in Fig. 4(a). Most importantly, one observes strong *suppression of spectral weight* at E_F and a peak of the signal at ∼1 eV below (not seen at the plain SiC:H surface [15]). Its roll-off to deeper binding energies may include intensity from the two further surface bands, and the signal at ∼2.4 eV relates to a cut of the bulk bands for this photon energy (see also Fig. S1 [13]). Importantly, this leaves the gapped region of interest towards the Fermi level unaffected.

For this spectrum, the Coulomb correlation U must be considered: It can result in a Mott-insulating state, where lower and upper Hubbard bands are separated by a gap comparable to U, as in Fig. 4(b). By definition, this effect is not included in the DFT picture of Fig. 3(b). The photoemission spectral features clearly argue for a Mott-insulating state. They bear a close resemblance to what is observed for $\sqrt{3}$-Sn on Si(111) [3]. However, there the peak of the lower Hubbard band is just ∼0.4 eV below E_F, while in the current system it is as low as ∼1 eV, which implies a U value of ∼2 eV.

We add that the only other adatom system known on SiC (0001) is the self-induced formation of a $\sqrt{3}$ reconstruction by (low-Z) Si, via mobile substrate atoms [9]. Photoemission data also suggest a Mott-insulating case [16,17], and U values around 1.6–2.1 eV were inferred [18,19].

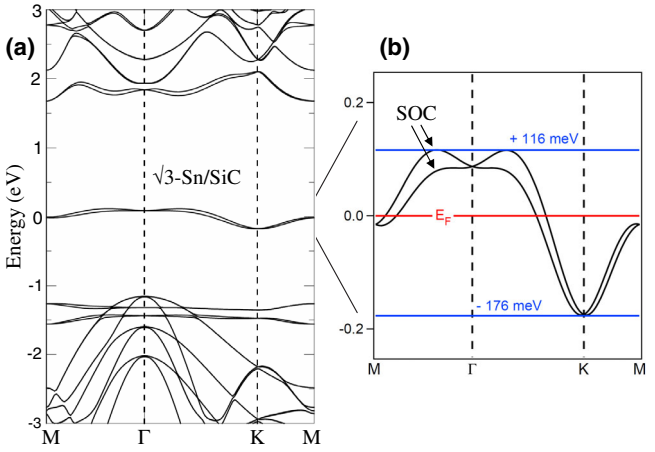

FIG. 3 (color online). (a) Band structure of $\sqrt{3}$-Sn on 4H-SiC(0001) from DFT including SOC. (b) Close-up of the Sn DB band at E_F, which (without U) is metallic and has a very narrow bandwidth of only ∼0.29 eV. SOC induces a notable band splitting.

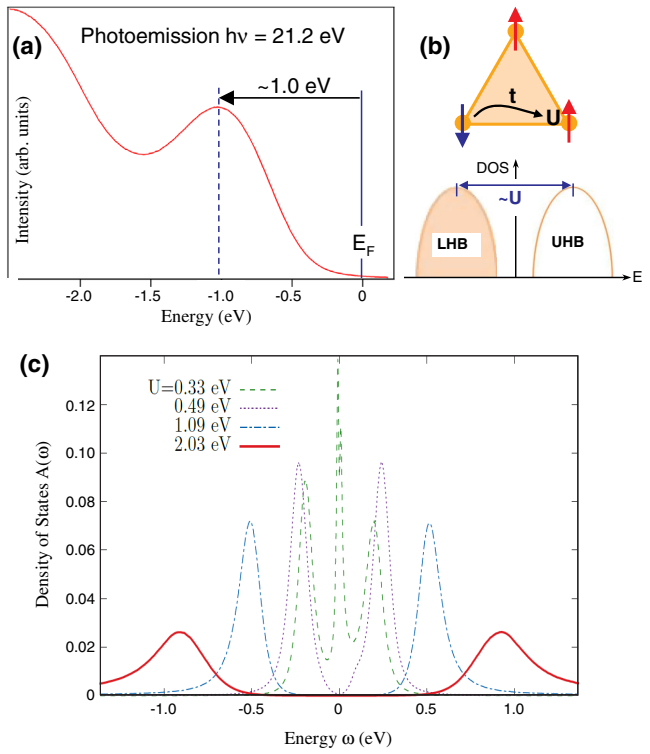

FIG. 4 (color online). (a) Experimental spectral function obtained from photoemission (He-I excitation, 300 K). The system is in an insulating state with a half-gap of ∼1.0 eV. (b) Coulomb correlations (U) with hopping (t) split the metallic DB state into lower and upper Hubbard bands (LHB and UHB, respectively). (c) Spectral function from DMFT, requiring high U values to approximate the experimental spectrum.

Role of the SiC substrate: Hopping and screening.—Based on a 20% reduced adatom spacing in SiC(0001) vs Si(111), one would expect both the hopping parameter and bandwidth of the DB to be increased. However, the contrary is the case: The LDA bandwidth of ∼0.50 eV in Sn/Si shrinks to ∼0.29 eV in Sn/SiC. This highlights the prominent role of the substrate and indicates that indirect hopping through it must be considered, as noted for Si(111) [20]. The low *effective* hopping across SiC relates to its higher "chemical inertia" compared to Si and Ge, owed to a partly ionic character (different electronegativities of Si and C), where the adatom-substrate hybridization is much reduced (see the charge contour in Fig. S2 [13]). In a single-band tight-binding model, we find that the *nearest-neighbor hopping amplitude* reduces from $t = 52.7$ meV for Sn on Si(111) [21] to $t = 27.3$ meV for the same adatoms on SiC(0001).

A second key effect is that 4*H*-SiC as a wide-gap (3.2 eV) substrate provides a substantially lower dielectric screening, which implies a larger U at the adatom. Relevant in dynamic screening is only the electronic (high-frequency) contribution. For Si, the electronic dielectric constant is $\varepsilon_\infty(\mathrm{Si}) \sim 11.7$, while for SiC it is only $\varepsilon_\infty(\mathrm{SiC}) \sim 6.5$ [22], which reduces the screening by a factor of ∼2.

Thus, the outstanding characteristics of the SiC substrate are twofold: (i) It renders the hopping small and therefore the DB band flat, and (ii) the small dielectric constant attenuates the screening of the local Coulomb interaction U. Together, this significantly boosts the electronic correlations: With $U = 0.66$ eV (Si) and $U \sim 2$ eV (SiC), one arrives at $U/t = 12.5$ for Si and a very large value of $U/t \sim 73$ for SiC.

Dynamic mean-field theory (DMFT).—We examined these correlations in Sn/SiC by a LDA + DMFT study [23], where the tight-binding model is subjected to an on-site Coulomb repulsion. Figure 4(c) shows the DOS of this surface band. The intensity at E_F is gradually lost with the increase of U, signaling a metal-insulator transition. Thus, strong Coulomb repulsion will certainly be a key ingredient to drive the system to an insulating ground state. For $U \sim 2$ eV we find qualitative agreement with the photoemission behavior; i.e., the peak for the lower Hubbard band is shifted to $\sim U/2 = 1$ eV below E_F.

Long-range interactions and magnetic ordering.—We point out that strong next-nearest-neighbor (NNN) hopping in the tight-binding picture is a characteristic feature of both Sn/Si and Sn/SiC, which can promote magnetic order. Strong NNN hopping is vital to explain the collinear AFM ordering of Sn/Si(111) in the presence of Coulomb interactions [3]. A DFT study in large supercells for that system [20], including substrate interaction with NNN hopping, likewise finds collinear AFM.

In this spirit, for Sn/SiC we compared the total energy of various magnetic configurations. Our spin-polarized calculations in a (3×6) unit cell are compatible with all four magnetic structures, i.e., ferromagnetism, ferrimagnetism, 120° AFM, and collinear AFM (not considering interactions beyond LDA, or SOC). The results in Table I show that also here collinear AFM is the most stable configuration.

TABLE I. Total energy [in units of meV per $(\sqrt{3} \times \sqrt{3})$ unit cell] of four different magnetic structures in Sn/SiC relative to the nonmagnetic ground state.

Magnetic configuration	Total energy per unit cell
Ferromagnetism	+3.03 meV
Ferrimagnetism	−2.03 meV
120° AFM	−2.75 meV
Collinear AFM	−2.93 meV

Since collinear AFM, 120° AFM, and ferrimagnetism are nearly energy degenerate, this leads to the exciting question whether a *spin liquid* may be encountered [24]. However, in our (noncorrelated) DFT calculation of the DOS for collinear AFM, the energy gap between occupied and empty states is merely $\Delta \sim 0.10$ eV, in stark contrast to the ∼2 eV deduced from experiment. This further underpins the role of strong Coulomb correlations, as in our LDA + DMFT results. Interestingly, as argued above, they may enhance the stability of collinear AFM [3].

Competing orders.—Nonlocal interactions (i.e., charge fluctuations) in triangular lattices on Si(111) were found by GW + DMFT to give rise to screening corrections, and charge ordering can set in [25]. This is also explored theoretically in Ref. [26], and experimental evidence in Sn/Ge(111) has been reported [27]. Its characteristic (3×3) superstructure can be experimentally distinguished from collinear AFM with its threefold degenerate $(2\sqrt{3} \times 2\sqrt{3})$ pattern [3]. Charge and spin order on the triangular lattice may even coexist [28], calling for a critical test on SiC at low temperature.

Coexistence of SOC and correlations.—Compared to the correlation strength, SOC is a small energy scale. However, in relation to the energy scale of the spin system, substantial SOC will leave its fingerprint on the magnetic pattern, due to pronounced breaking of the SU(2) symmetry. SOC in the presence of correlations thus serves to enrich the arena of frustrated magnetism. In the strong coupling (large U) limit, where magnetism develops on the triangular lattice, SOC leads to anisotropic spin exchange couplings that will, e.g., deform the 120° Néel order [5]. As another possibility, a quantum compass model can be stabilized, as proposed for triangular transition metal oxides [6]. Assuming significant easy-axis anisotropy, unprecedented phases and phase transitions might also be identified, as triggered by external magnetic fields [29]. For intermediate U, in a nonmagnetic insulator regime where the Mott gap has already developed but charge fluctuations are still significant, a spin liquid might be found (see, e.g., Ref. [30] and references therein).

Large SOC combined with interaction effects may also suffice to induce band inversion and generate a topological insulator (TI), albeit that this is contingent on the lattice symmetry. In bulk α-Sn (diamond lattice), SOC drives the formation of a TI [31]. Moreover, theoretically, a high-Z triangular lattice on a (111) diamond-type substrate can host a TI state [32].

In conclusion, we have demonstrated a pathway to fabricate high-Z artificial atom lattices on SiC(0001). A triangular lattice of Sn atoms exhibits unexpectedly strong Coulomb correlations. Our theoretical analysis, which also finds enhanced SOC, allows us to explain this by reduced screening and suppressed hopping, both mediated by the "chemistry" of the SiC template. This emphasizes the prominent role of the (wide-gap) substrate for generating electronically correlated adatom systems. These novel possibilities encourage further exploration of Sn-based lattices on SiC.

This work was supported by the Deutsche Forschungsgemeinschaft (FOR 1162), and G. L., W. H., R. T. by the European Research Council (ERC-StG-Topolectrics-336012). We acknowledge computational time at the Jülich Supercomputing Centre and on the GCS Supercomputer SuperMUC at Leibniz Supercomputing Centre (LRZ).

*joerg.schaefer@physik.uni-wuerzburg.de

[1] S. Modesti, L. Petaccia, G. Ceballos, I. Vobornik, G. Panaccione, G. Rossi, L. Ottaviano, R. Larciprete, S. Lizzit, and A. Goldoni, Phys. Rev. Lett. **98**, 126401 (2007).
[2] R. Cortés, A. Tejeda, J. Lobo, C. Didiot, B. Kierren, D. Malterre, E. G. Michel, and A. Mascaraque, Phys. Rev. Lett. **96**, 126103 (2006).
[3] G. Li, P. Höpfner, J. Schäfer, C. Blumenstein, S. Meyer, A. Bostwick, E. Rotenberg, R. Claessen, and W. Hanke, Nat. Commun. **4**, 1620 (2013).
[4] P. Höpfner *et al.*, Phys. Rev. Lett. **108**, 186801 (2012).
[5] X.-Y. Feng, X. Dong, and J. Dai, Phys. Rev. B **84**, 212406 (2011).
[6] G. Jackeli and G. Khaliullin, Phys. Rev. Lett. **102**, 017205 (2009).
[7] W. Witczak-Krempa, G. Chen, Y. B. Kim, and L. Balents, Annu. Rev. Condens. Matter Phys. **5**, 57 (2014).
[8] K. V. Emtsev *et al.*, Nat. Mater. **8**, 203 (2009).
[9] V. Ramachandran and R. M. Feenstra, Phys. Rev. Lett. **82**, 1000 (1999).
[10] S. Glass *et al.* (to be published).
[11] G. Kresse and J. Hafner, Phys. Rev. B **47**, 558 (1993);
G. Kresse and J. Furthmüller, Comput. Mater. Sci. **6**, 15 (1996).
[12] For DFT: energy cutoff of 400 eV, atomic relaxation until forces $<10^{-3}$ eV/Å at fixed experimental lattice constant $a = 3.073$ Å [Y. Goldberg *et al.*, in *Properties of Advanced Semiconductor Materials*, edited by M. E. Levinshtein *et al.* (Wiley, New York, 2001), p. 93], and a $21 \times 21 \times 1$ Monkhorst-Pack grid in the Brillouin zone.
[13] See Supplemental Material at http://link.aps.org/supplemental/10.1103/PhysRevLett.114.247602 for additional information on the atomic and electronic structure of the Sn atom lattice on SiC.
[14] J. Tersoff and D. R. Hamann, Phys. Rev. B **31**, 805 (1985).
[15] K. V. Emtsev, Th. Seyller, L. Ley, L. Broekman, A. Tadich, J. D. Riley, R. G. C. Leckey, and M. Preuss, Phys. Rev. B **73**, 075412 (2006).
[16] J. Furthmüller, F. Bechstedt, H. Husken, B. Schroter, and W. Richter, Phys. Rev. B **58**, 13712 (1998).
[17] R. Ostendorf, K. Wulff, C. Benesch, H. Merz, and H. Zacharias, Phys. Rev. B **70**, 205325 (2004).
[18] J. E. Northrup and Jörg Neugebauer, Phys. Rev. B **57**, R4230 (1998).
[19] M. Rohlfing and J. Pollmann, Phys. Rev. Lett. **84**, 135 (2000).
[20] J.-H. Lee, X. Y. Ren, Y. Jia, and J. H. Cho, Phys. Rev. B **90**, 125439 (2014).
[21] G. Li, M. Laubach, A. Fleszar, and W. Hanke, Phys. Rev. B **83**, 041104(R) (2011).
[22] L. Patrick and W. J. Choyke, Phys. Rev. B **2**, 2255 (1970).
[23] G. Kotliar, S. Y. Savrasov, K. Haule, V. S. Oudovenko, O. Parcollet, and C. A. Marianetti, Rev. Mod. Phys. **78**, 865 (2006).
[24] S. Nakatsuji *et al.*, Science **309**, 1697 (2005).
[25] P. Hansmann, T. Ayral, L. Vaugier, P. Werner, and S. Biermann, Phys. Rev. Lett. **110**, 166401 (2013).
[26] G. Santoro, S. Scandolo, and E. Tosatti, Phys. Rev. B **59**, 1891 (1999).
[27] R. Cortés, A. Tejeda, J. Lobo-Checa, C. Didiot, B. Kierren, D. Malterre, J. Merino, F. Flores, E. G. Michel, and A. Mascaraque, Phys. Rev. B **88**, 125113 (2013).
[28] S. Zhou and Z. Wang, Phys. Rev. Lett. **98**, 226402 (2007).
[29] D. Yamamoto, G. Marmorini, and I. Danshita, Phys. Rev. Lett. **112**, 127203 (2014).
[30] M. Laubach *et al.*, arXiv:1401.8198v2.
[31] A. Barfuss *et al.*, Phys. Rev. Lett. **111**, 157205 (2013).
[32] Q.-F. Liang *et al.*, arXiv:1407.7320v1.